TITLE PAGE

Citation Format:

Wabnitz, H., Taubert, D.R., Funane, T., Kiguchi, M., Eda, H., Pifferi, A., Torricelli, A., Macdonald, R. "Characterization of homogeneous tissue phantoms for performance tests in diffuse optics" (2016) Progress in Biomedical Optics and Imaging - Proceedings of SPIE, 9700,

Copyright notice:

DOI abstract link:

http://dx.doi.org/10.1117/12.2209038

Characterization of homogeneous tissue phantoms for performance tests in diffuse optics

Heidrun Wabnitz*[a], Dieter Richard Taubert[a], Tsukasa Funane[b], Masashi Kiguchi[b], Hideo Eda[c], Antonio Pifferi[d,e], Alessandro Torricelli[d,e], Rainer Macdonald[a]

[a]Physikalisch-Technische Bundesanstalt (PTB), Abbestraße 2-12, 10587 Berlin, Germany; [b]Hitachi Ltd., Research & Development Group, Hatoyama, Saitama 350-0395, Japan; [c]The Graduate School for the Creation of New Photonics Industries, 1955-1, Kurematsu, Nishi-ku, Hamamatsu, Shizuoka 431-1202, Japan; [d]Politecnico di Milano, Dipartimento di Fisica, Piazza Leonardo da Vinci 32, 20133 Milano, Italy; [e]Istituto di Fotonica e Nanotecnologie, CNR, Piazza Leonardo da Vinci 32, 20133 Milano, Italy

ABSTRACT

Solid homogeneous turbid phantoms can be employed to mimic the attenuation and angular distribution of light emerging from tissue, e.g., to assess the responsivity of the detection system of diffuse optics instrumentation and to support standardized performance tests of functional near-infrared spectroscopy devices. We present three methods to quantify the wavelength-dependent diffuse transmittance, relying on (1) measurement of radiance exiting the phantom by a detector far from the exit aperture, (2) simple recording of radiance by a power meter close to the exit aperture and correction for the finite distance between phantom surface and detector, (3) determination of the reduced scattering and absorption coefficients by time-resolved diffuse transmittance measurements and forward calculation of the time-integrated diffuse transmittance based on the diffusion model. The implications of the different approximations related to these approaches are discussed. The various methods were applied to characterize solid slab phantoms, and the results were compared. Specifically, for an epoxy-resin based phantom having a thickness of 2 cm, a reduced scattering coefficient of about 0.5/mm and an absorption coefficient of about 0.01/mm, the diffuse transmittance values obtained by the three different methods were found to agree within about 10%.

Keywords: tissue-like phantoms, performance characterization, time-domain diffuse optical spectroscopy, functional near-infrared spectroscopy, standardization

1. INTRODUCTION

Performance characterization and validation and standardization of instruments for biomedical optical imaging and spectroscopy necessitate phantoms that mimic relevant aspects of the tissue under investigation[1,2]. Basic requirements for phantoms for diffuse optical imaging and spectroscopy of organs like brain and breast are a realistic, strong diffuse light attenuation as well as a nearly Lambertian angular characteristic of the exiting radiation. Both requirements can be met with solid homogeneous turbid phantoms of suitable dimensions and optical properties. Apart from serving as test objects for the quantification of the reduced scattering and absorption coefficients as detailed in the MEDPHOT protocol[3], they can mimic the diffuse attenuation in tissues[4].

When dealing with diffuse optics, the detection efficiency of a system is not only related to the detector quantum efficiency and to losses in the optical system, but also to the overall light collection efficiency determined by the detector area and the acceptance angle of the optical system. These aspects were included in an extended definition of responsivity to encompass diffuse optics systems[4]. Solid homogeneous phantoms can be useful to realize a uniform diffuse light source with known photon radiance and approximately Lambertian angular emission characteristics that can be employed to measure the responsivity of the detection system of instruments in diffuse optics. This approach was applied to compare the detection efficiency of a number of time-domain optical brain imagers of four research groups[4]. In this application, the detection was performed by time-correlated single photon counting, and therefore photon-related quantities were analyzed. However, an analogous approach to responsivity characterization can be used with continuous wave (CW) instrumentation. The relations given in the present work pave the way for such extension.

A particular need to characterize solid homogeneous phantoms in terms of their attenuation arose in the context of the preparation of an IEC/ISO standard for functional NIRS equipment (IEC 80601-2-71:2015 [5]) where such phantoms, in part equipped with means to produce an intensity change, are stipulated for various performance tests. When determining the amount of light that exits a phantom it is important to specify the position and the size of the aperture area on the surface of the phantom and to take into account a potential clipping of the angular distribution by the detector. With these factors considered, it is possible to estimate the diffuse transmittance of a phantom in a straightforward measurement by means of a power meter. We support this conclusion by comparing the results of such measurements with those of other approaches to quantify diffuse transmittance.

2. THEORETICAL BACKGROUND

The homogeneous phantoms discussed in the following are made of highly scattering and weakly absorbing materials (reduced scattering coefficient $\mu_s' \sim 10\ \mathrm{cm}^{-1}$, absorption coefficient $\mu_a \leq 0.1\ \mathrm{cm}^{-1}$) of dimensions of several centimeters (thickness $d \geq 2$ cm, lateral dimensions ≥ 10 cm). In this case, light propagation is essentially diffusive. Light injection is accomplished by an approximately point-like source. After diffuse propagation through the phantom, light can exit on any location on the phantom surface. In the following, we assume a parallel slab geometry and consider the light exiting the surface through a small area A opposite to the injection point.

The light exiting the phantom after diffuse propagation can be modeled by a Lambertian source[6,7] with radiance L. The $\cos\Theta$ angular distribution (Θ - angle between the propagation direction of exiting photons and the surface normal) is a reasonable approximation in the diffusion regime and for a ratio >1 of the refractive indices inside and outside the turbid medium. The wavelength-dependent radiance $L(\lambda)$ can be related to the input power $P_{in}(\lambda)$ via a phantom-specific wavelength-dependent diffuse transmittance factor $\kappa(\lambda)$ (in $\mathrm{m}^{-2}\mathrm{sr}^{-1}$),

$$L(\lambda) = \kappa(\lambda)\, P_{\mathrm{in}}(\lambda)\,. \tag{1}$$

Note that this equation is equivalent to Eq. (3) in Ref. 4 for photon-related quantities (κ_p in $\mathrm{W}^{-1}\mathrm{s}^{-1}\mathrm{m}^{-2}\mathrm{sr}^{-1}$).

The total power of light that exits a small aperture of area A on the phantom surface, opposite to the point of light injection, in any direction is

$$P_{\mathrm{out,tot,\,A}}(\lambda) = \pi\, L(\lambda)\, A = \pi\, \kappa(\lambda)\, A\, P_{\mathrm{in}}(\lambda)\,. \tag{2}$$

The factor π results from the solid angle integration over the full hemisphere assuming a Lambertian distribution. The (time-integrated) spatially resolved diffuse transmittance T (in m^{-2}) is related to the total amount of light exiting into the half space per unit area,

$$T = P_{\mathrm{out,tot,\,A}} \,/\, A \,/\, P_{\mathrm{in}}\,. \tag{3}$$

Thus the relationship between T and κ is

$$T(\lambda) = \pi\, \kappa(\lambda)\,. \tag{4}$$

Optical loss (in dB) is another quantity used to describe the diffuse attenuation of a turbid phantom. It is not a unique characteristic of the phantom but rather depends on the area of the exit aperture and the fraction of the angular distribution of the outgoing radiation that reaches the detector. Assuming that the full distribution is detected, i.e. the radiation exiting the aperture into the half space at any angle Θ, the optical loss is given by

$$OL = -10\log_{10}\left(P_{\mathrm{out,tot,\,A}} / P_{\mathrm{in}}\right) = -10\log_{10}\left(A\,T\right)\,. \tag{5}$$

A detector centered with respect to the aperture on the surface of the phantom cannot collect the total diffuse output power, due to the limited (circular) sensor area $\pi\, r_{pow}^2$ and its finite distance from the surface. To avoid an underestimation of T, a correction factor K_{pow} (> 1) can be derived from the radiant power transfer equation[8],

$$K_{\mathrm{pow}} = P_{\mathrm{out,tot,\,A}} / P_{\mathrm{pow}} = \frac{r_A^2 + r_{\mathrm{pow}}^2 + a^2 + \sqrt{\left(r_A^2 + r_{\mathrm{pow}}^2 + a^2\right)^2 - 4 r_A^2 r_{\mathrm{pow}}^2}}{2 r_{\mathrm{pow}}^2}\,, \tag{6}$$

where P_{pow} is the power recorded by the detector (power meter), r_{pow} the radius of its photosensitive area, a its distance from the phantom surface, and r_A the radius of the circular aperture of area A on the phantom surface (see insert of Fig. 1). The light distribution across the aperture as well as the responsivity across the detector are assumed to be uniform.

The behavior of the correction factor as a function of a is illustrated in Fig. 1. The simulations show that K_{pow} becomes relevant as soon as a is no longer negligible in comparison to r_{pow}, and also if $r_A > r_{pow}$. The following special cases are worth considering: In the (unrealistic) case $a = 0$, no correction is necessary ($K_{pow} = 1$) as long as r_A remains smaller than r_{pow}, otherwise $K_{pow} = r_A^2/r_{pow}^2$. In the limit $a >> r_A, r_{pow}$ we have $K_{pow} = a^2/r_{pow}^2$.

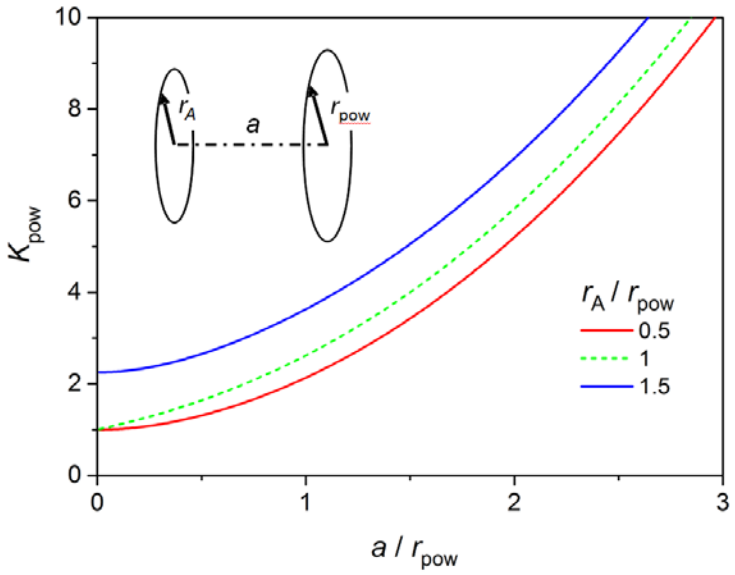

Figure 1. Correction factor K_{pow} as a function of distance a for various ratios r_A/r_{pow}

3. MEASUREMENTS OF DIFFUSE TRANSMITTANCE

The most common method to measure diffuse transmittance of a turbid sample employs an accurately calibrated integrating sphere setup. However, with this method the sample thickness is usually limited to a few mm. Moreover, such equipment is not easily accessible to each lab. Therefore, we focused on the three approaches illustrated in Fig. 2.

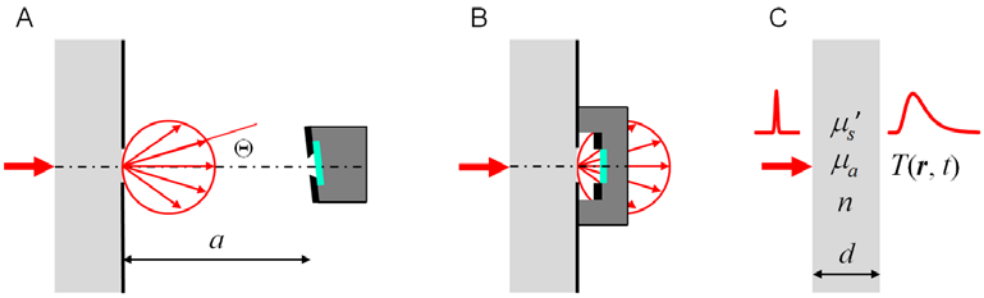

Figure 2. Schematic of three methods to derive diffuse transmittance of a turbid phantom

A Detection far from the phantom surface

A calibrated detector is placed far from the aperture on the phantom surface, with $a >> r_A, r_{pow}$. The radiation is measured in a small solid angle around the optical axis. In this way, L is obtained primarily. By rotating the detector arrangement around the center of the exit aperture (angle Θ), the angular distribution of the radiation exiting the surface can be recorded additionally.

This method was implemented for the characterization of responsivity phantoms as described in Ref. 4 in detail. It relied on the use of a Si photodiode-aperture combination with calibrated spectral irradiance responsivity. The radius of the aperture on the phantom was 2.5 mm, the aperture in front of the photodiode had a radius of 4 mm, and the distance a between them

was 92 mm. The detector was slightly tilted (5°) to avoid that light reflected from the photodiode could reach the phantom through the aperture again. The photocurrent (several nA) was recorded by a picoamperemeter.

B Detection close to the phantom surface

This straightforward method employs a power meter with a sensitive photodiode detector to measure the integral power impinging on the sensor. The closer the sensor head is placed to the phantom, the higher is the recorded power. To obtain an estimate of the total diffuse radiation emitted from the phantom through the aperture on its surface, the correction according to Eq. (6) has to be applied. Compared to method (A), a much larger fraction of the total radiation exiting the aperture is collected which reduces the requirements regarding the detector sensitivity. It should be noted that a possible influence of radiation reflected from the sensor back to the phantom has to be considered.

The measurements were performed with a power meter Fieldmaster (Coherent) with the sensor head LM-2. This power meter was selected because of its linearity and stability down to several nW. The input power of a few mW was measured with the same sensor. Moreover, the surface of this sensor appeared bluish and had a low reflectivity in the red and near-infrared spectral ranges. The fraction of a nearly perpendicularly impinging laser beam that was reflected was measured to be 8% (650 nm). The exposed photosensitive area had a diameter of $2r_{pow}$ = 7.9 mm and was located at a depth of a_{min} = 7.4 mm from the front face of the housing. The aperture on the surface of the phantom was made of a thin (50 µm) matte black aluminum foil (BKF12, Thorlabs) in which a cylindrical aperture of radius r_A = 3.75 mm was cut out.

Two different light sources were used, (1) a picosecond diode laser (Sepia II, Picoquant GmbH, Germany) with a laser head operating at 650 nm and (2) the supercontinuum laser with AOTF described in the next section.

C Diffuse transmittance derived from the optical properties of the phantom

The diffuse transmittance of a solid diffusive phantom is mainly determined by the bulk optical properties of the material, i.e., μ_s', μ_a and refractive index n. Based on solutions of the diffusion equation for light propagation in homogeneous turbid media for the appropriate geometry, the diffuse (CW) transmittance can be estimated.

The optical properties were determined by time-resolved measurements. A supercontinuum laser (SC500-6, Fianium Ltd, UK) equipped with an 8-channel acousto-optic tunable filter (AOTF) for the near-infrared spectral range provided picosecond pulses (< 100 ps) at a repetition rate of 40.5 MHz. It provided an output power of several mW employing a single AOTF channel when tuned to 690 nm, 750 nm or 830 nm. For the measurements at 650 nm, 5 channels were stacked together to achieve a similar output power. The light was delivered to the phantom by a multimode fiber (diameter 200 µm, NA 0.22, length 2 m). Another fiber (diameter 550 µm, NA 0.22, length 1 m) (both from Thorlabs) collected the light from the phantom. The detector was a hybrid detector module HPM 100-50 (Becker&Hickl GmbH, Germany). Distributions of time of flight (DTOF) of detected photons were recorded by a time-correlated single photon counting (TCSPC) module (SPC-150, Becker&Hickl, Germany). The time resolution (FWHM of the instrument response function, IRF) was about 170 ps.

The measurements were performed in transmission geometry with a detector offset of 0, ±1 cm and ±2 cm as well as in reflection geometry at a source-detector separation of 2 cm, 3 cm and 4 cm. The optical properties were derived by fitting each individual measured DTOF with the appropriate analytical solution of the photon diffusion equation with extrapolated boundary conditions[9], convolved with the measured IRF. The fit parameters were μ_s' and μ_a while the time origin was fixed. An amplitude factor was determined from the ratio of the integral for the measured and theoretical curves in each iteration step. The fit range extended from 80% of the maximum of the DTOF on the leading edge down to 0.1% on the trailing edge. For homogeneous media the measurements with all geometrical options mentioned above are expected to yield essentially the same results. Substantial inconsistencies can be an indication of inhomogeneities of the material or of non-adequacy of the diffusion model. It should be noted that the estimation of μ_s' and μ_a for method C solely relies on the temporal profile of the time-of-flight distribution and does not depend on any amplitude information. Once the optical properties are determined, they are employed to estimate the CW (or time-integrated) diffuse transmittance by a forward calculation based on the diffusion model and extrapolated boundary conditions.

D Phantom

All three methods presented before were applied to one of the responsivity phantoms (“2o”) described and characterized in Ref. 4. It was a cylindrical slab of thickness 2 cm and diameter 10.5 cm, made of epoxy resin with TiO_2 particles added as a scattering medium and black toner as an absorbing medium, following the recipe published by Swartling et al.[10]. The refractive index n of these phantoms was assumed to be 1.55.

4. RESULTS AND DISCUSSION

A first test of method B included the recording of the distance dependence of power detected by the power meter. A result is shown in Fig. 3. The diameter of the aperture on the surface of phantom "2o" was $2r_A = 7.5$ mm. The sensor head was centered with the center of the aperture. The input power from the diode laser was 2 mW (650 nm), the output detected by the power meter dropped from 810 nW in the closest position when the sensor head was touching the aperture foil to 28 nW at the farthest position. Both the measured values and the simulation were normalized at the same distance. The measured distance dependence matches well with the function predicted by the radiant transfer equation. The correction given by Eq. (6) corresponds to an extrapolation of this dependence to $a = 0$. Since $r_A > r_{pow}$, this extrapolated power is equal to the total exiting power. It is approximately 5 times larger than the power measured at the closest position, i.e. ~4 µW. With $A = 44.2$ mm^2 and applying Eq. (3), a transmittance of T~45 m^{-2} results.

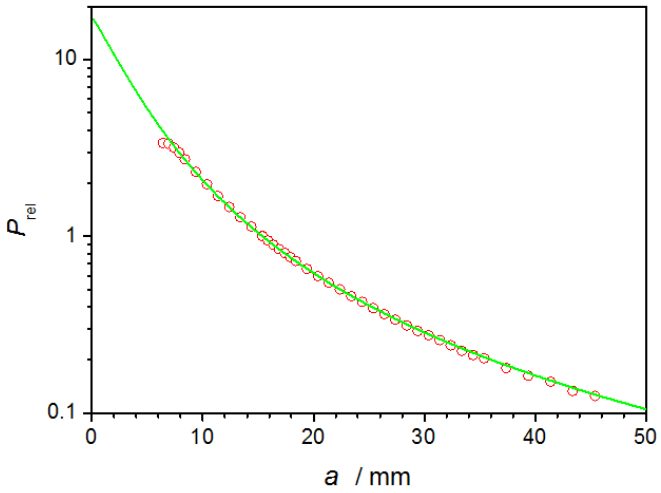

Figure 3. Detected relative power as a function of distance a between the surface of phantom "2o" and the photosensor of the power meter, circles – measurement, line – simulation based on the radiant transfer equation.

A comparison of methods A and B is provided in Fig. 4. The results for method A are taken from the same measurement that was presented in Fig. 2 of Ref. 4 to characterize five responsivity phantoms in terms of their wavelength-dependent photon transmittance factor κ_p (in W^{-1}s^{-1}m^{-2}sr^{-1}). Note that in Fig. 4 the transmittance factor κ (in m^{-2}sr^{-1}) is plotted. The left and right axes (κ and T) are linked by Eq. (4). A third axis is added to illustrate the description of diffuse transmittance in terms of the "optical loss" as defined in Eq. (5).

The agreement between the results of both measurements is striking. Provided that the centers of sensor head and aperture on the phantom are laterally well aligned, the most critical parameter determining the uncertainty of method B is the distance between surface and photosensor, as can be inferred from Fig. 3. The error bars were obtained with a rather conservative estimate of the uncertainty of the distance a of ±0.2 mm. A small offset in λ was introduced to avoid overlapping symbols.

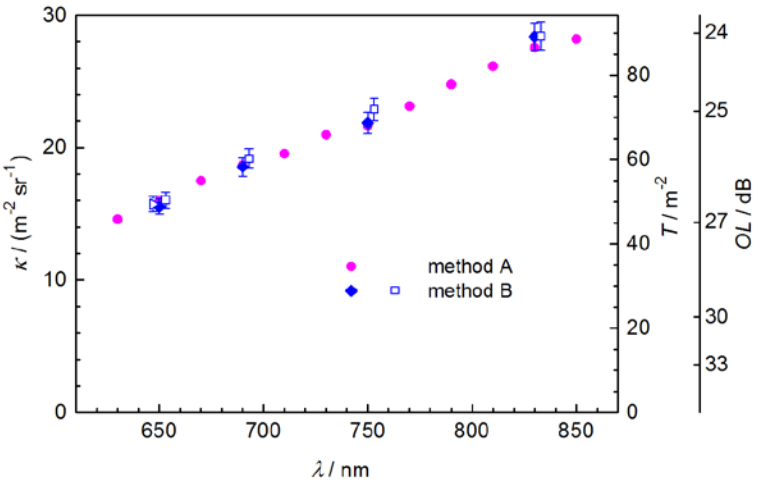

Figure 4. Wavelength dependence of the diffuse transmittance factor κ, diffuse transmittance T and optical loss OL for the phantom "2o". Diamonds and squares: two independent measurements, triangle: measurement with diode laser.

For method C, the optical properties were determined from time-resolved measurements. The results presented in Fig. 5a show a reduced scattering coefficient that is decreasing with increasing wavelength as expected for turbid materials of this kind.[3] The absorption coefficient remains rather constant. The measurements at the various detector offsets provided largely consistent results, as represented by the error bars. Note that they represent the standard deviation of the distribution of 6 values measured rather than the uncertainty of the mean. The filled and open symbols correspond to independent sets of measurements, illustrating the good reproducibility. Based on all pairs of optical properties, the CW diffuse transmittance was calculated, again with extrapolated boundary conditions. The results are shown in Fig. 5b, superimposed on the results obtained by method A. The value at 750 nm completely overlaps with the result from method A, while the transmittance values at 650 nm and 830 mm are slightly larger or smaller, respectively, than those obtained from method A. Nevertheless, the correspondence is surprisingly good – deviations remain within about 10% – given the more complex indirect calculation.

The results of measurements according to methods B and C on various phantoms made from semimanufactured polyoxymethylene (POM) plastic turned out to be less consistent (data not shown). The most likely reason was the heterogeneity of these phantom blocks that exhibited a denser appearance near the center plane of the plate material used. This feature seems to be a common consequence of the manufacturing process of molding.

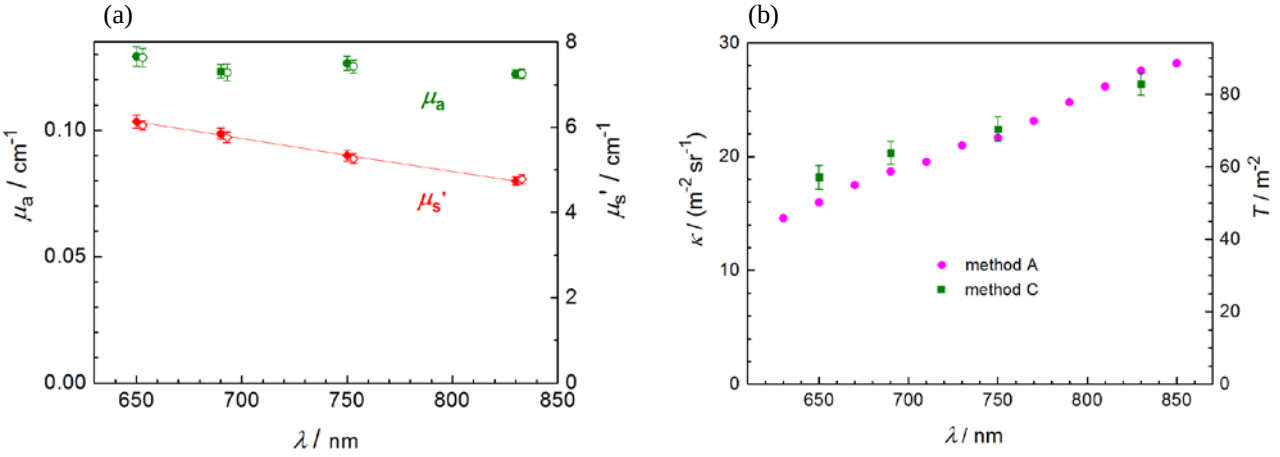

Figure 5. (a) Optical properties of phantom "2o" (mean and standard deviation) obtained from time-resolved measurements in transmission geometry for the detector offsets 0 (measured twice), ±1 cm and ±2 cm, μ_a – circles, μ_s' - diamonds. Filled and open symbols represent independent sets of measurements, an offset in λ was introduced to avoid overlapping.
(b) Comparison with method A.

5. CONCLUSIONS

Although much simpler than method A, method B is well suited to estimate diffuse transmittance of a turbid phantom, provided that a correction is applied that accounts for the finite distance between the surface of the phantom and the photodetector. Both methods were compared on the example of a previously well characterized phantom. The critical factors that could lead to a disagreement between the two methods are a deviation from the Lambertian emission characteristic, uncertainties in the geometrical parameters, insufficient linearity of the power meter and a finite reflectivity of the power meter sensor. A reflection coefficient of less than 10% can obviously be tolerated without correction. For highly reflecting sensors the necessity of a related correction has to be considered. Method B is limited to not too thick phantoms, so as to stay within the measuring range of the power meter.

A good agreement between the photometric methods A and B on one hand and method C, that relies on the knowledge of the bulk optical properties of the phantom, on the other hand is much less obvious. It depends on the homogeneity of the material that is an important prerequisite for reliable fit results. Moreover, the surface roughness of the sample is expected to affect the diffuse transmittance as well as the angular distribution of the radiation exiting the phantom. In case of phantom "2o" that had a smooth but still matte surface the diffusion model with extrapolated boundary condition was evidently a valid description. However, this finding cannot simply be generalized, and the influence of surface roughness necessitates further studies.

The applicability of the diffusion approximation is limited to thick, highly scattering and weakly absorbing phantoms. In other cases, alternative models to describe light propagation, i.e. Monte Carlo approaches or the radiative transfer equation can be employed. Surely, method C is not straightforward, requiring particular experience in accurate time-resolved diffuse optical measurements and their analysis. Also, the uncertainties of the estimates of μ_s' and μ_a can severely affect the results. On the other hand, method C can be easily applied by non-expert users adopting phantoms with certified optical properties.

REFERENCES

[1] Pogue, B. W., Patterson, M. S., "Review of tissue simulating phantoms for optical spectroscopy, imaging and dosimetry," J. Biomed. Opt. 11(4), 041102 (2006).

[2] Hwang, J., Ramella-Roman, J. C., Nordstrom, R., "Introduction: feature issue on phantoms for the performance evaluation and validation of optical medical imaging devices," Biomed. Opt. Express 3(6), 1399–1403 (2012).

[3] Pifferi, A., Torricelli, A., Bassi, A., Taroni, P., Cubeddu, R., Wabnitz, H., Grosenick, D., Möller, M., Macdonald, R., et al., "Performance assessment of photon migration instruments: the MEDPHOT protocol," Appl. Opt. 44(11), 2104–2114 (2005).

[4] Wabnitz, H., Taubert, D. R., Mazurenka, M., Steinkellner, O., Jelzow, A., Macdonald, R., Milej, D., Sawosz, P., Kacprzak, M., et al., "Performance assessment of time-domain optical brain imagers, part 1: basic instrumental performance protocol," J. Biomed. Opt. 19(8), 086010 (2014).

[5] "IEC 80601-2-71:2015 | IEC Webstore.", <https://webstore.iec.ch/publication/22638> (23 January 2016).

[6] Kienle, A., Lilge, L., Patterson, M. S., Hibst, R., Steiner, R., Wilson, B. C., "Spatially resolved absolute diffuse reflectance measurements for noninvasive determination of the optical scattering and absorption coefficients of biological tissue," Appl. Opt. 35(13), 2304–2314 (1996).

[7] Kienle, A., Foschum, F., "250 years Lambert surface: does it really exist?," Opt. Express 19(5), 3881–3889 (2011).

[8] Bass, M., DeCusatis, C., Enoch, J., Lakshminarayanan, V., Li, G., MacDonald, C., Mahajan, V., Stryland, E. V., Handbook of Optics, Third Edition Volume II: Design, Fabrication and Testing, Sources and Detectors, Radiometry and Photometry, 3 edition, McGraw-Hill Professional, New York (2009).

[9] Contini, D., Martelli, F., Zaccanti, G., "Photon migration through a turbid slab described by a model based on diffusion approximation. I. Theory," Appl. Opt. 36(19), 4587–4599 (1997).

[10] Swartling, J., Dam, J. S., Andersson-Engels, S., "Comparison of spatially and temporally resolved diffuse-reflectance measurement systems for determination of biomedical optical properties," Appl. Opt. 42(22), 4612–4620 (2003).